Mountains to climb: on the role of seamounts in upwelling of deep ocean waters

Ali Mashayek (mashayek@ic.ac.uk)
Imperial College London
Jonathan Gula
Université de Brest https://orcid.org/0000-0002-0876-9557
Lois Baker
Imperial College
Alberto Naveira Garabato
University of Southampton https://orcid.org/0000-0001-6071-605X
Laura Cimoli
University of California San Diego
James Riley
University of Washington

Article

Keywords:

Posted Date: October 25th, 2021

DOI: https://doi.org/10.21203/rs.3.rs-939198/v1

Mountains to climb: on the role of seamounts in upwelling of deep ocean waters through turbulent mixing

A. Mashayek[1], J. Gula[2,3], L.E. Baker[4], A. Naveira Garabato[5], L. Cimoli[6], and J. J. Riley[7]

[1,4]Imperial College London
[2]Univ Brest, CNRS, IRD, Ifremer, Laboratoire d'Océanographie Physique et Spatiale (LOPS), IUEM, Brest, France
[3]Institut Universitaire de France (IUF), Paris, France
[5]University of Southampton
[6]Scripps Institution of Oceanography
[7]University of Washington

2021

Ocean turbulent mixing exerts an important control on the rate and structure of the overturning circulation. Recent observational evidence suggests, however, that there could be a mismatch between the observed intensity of mixing integrated over basin or global scales, and the net mixing required to sustain the overturning's deep upwelling limb. Here, we investigate the hitherto largely overlooked role of tens of thousands of seamounts in resolving this discrepancy. Dynamical theory indicates that seamounts may stir and mix deep waters by generating lee waves and topographic wake vortices. At low latitudes, this is enhanced by a layered vortex regime in the wakes. We consider three case studies (in the equatorial zone, Southern Ocean and Gulf Stream) that are predicted by theory to be representative of, respectively, a layered vortex, barotropic wake, and hybrid regimes, and corroborate theoretical scalings of mixing in each case with a realistic regional ocean model. We then apply such scalings to a global seamount dataset and an ocean climatology to show that seamount-generated mixing makes a leading-order contribution to the global upwelling of deep waters. Our work thus brings seamounts to the fore of the deep-ocean mixing problem, and urges observational, theoretical and modeling efforts toward incorporating the seamounts' mixing effects in conceptual and numerical models of the ocean circulation.

Turbulence at centimetre scales plays a pivotal role in shaping the overturning circulation of the deep ocean (1; 2), as well as the ocean's capacity to distribute and store climate-critical tracers (3; 4). As dense deep water masses flow away from their high-latitude formation regions, small-scale turbulence induces mixing with surrounding layers, leading to a net transfer of water across isopycnals. These transfers regulate the rate and structure of deep-ocean overturning (5; 6; 7) and, in so doing, influence the oceanic inventories and turnover time scales of heat, carbon and other important biogeochemical substances.

After decades of extensive research, we now have a solid understanding of the key energy sources of turbulent mixing (winds, tides, and geothermal heating through the seafloor) (1; 8), and of a wide range of mechanisms of small-scale turbulence generation (9; 10). However, several major knowledge gaps remain. Possibly chief amongst them is the uncertain role of turbulent processes near the ocean's bottom boundary. These processes have been argued to potentially account for the bulk of deep-ocean upwelling (1; 2), but, with few targeted observations, comparatively little is known about their nature and large-scale impacts.

Most past investigations of turbulent mixing near the bottom boundary have examined contributions from either the breaking of internal waves (following the waves' generation, reflection or scattering at the boundary; see (9) for a recent review), or a range of complex non-wave processes in topographically-constrained canyons and passages (*e.g.*, hydraulic jumps at sills) (11; 12). More recently, the focus has shifted increasingly to a distinct class of phenomena underpinning near-boundary mixing: submesoscale instabilities (13; 14; 15; 16). These instabilities develop as quasi-geostrophic mesoscale flows over sloping topography generate a reversal in the sign of potential vorticity near the boundary, and induce overturning motions that restore stability by mixing boundary and off-boundary waters. Intense boundary mixing by submesoscale instabilities has been documented in association with strong mesoscale motions (such as the Gulf Stream (17) or a deep western boundary current (14)), suggesting that the instabilities may be widely active mixing agents.

Yet, as common as these instabilities might be, fresh theoretical advances emphasize the potential prevalence of a largely overlooked, more generic form of mesoscale flow-topography interaction, which encompasses and

transcends most scenarios of submesoscale instability development: the generation of topographic wakes. These wakes are produced when the highly-sheared near-boundary flow separates from sloping topography and moves into the oceanic interior (18). Flow separation needs not always be associated with a reversal in the sign of potential vorticity close to the boundary, but may be readily enabled by the boundary's geometry (19) or the background mesoscale strain field (20). Upon escaping the boundary's constraint, the separated, sheared flow undergoes a variety of instabilities, which lead to both elevated turbulent mixing in the wake (17; 21; 22) and the generation of submesoscale vortical filaments (19; 23; 24). These filaments often merge and align to form submesoscale coherent vortices (SCVs) and, ultimately, may result in further mixing via a secondary emission of internal waves.

Where, then, might we expect topographic wakes to induce vigorous turbulent mixing in the deep ocean? Although wake generation can potentially occur at any sloping topography, the most common form of such topography is provided by seamounts – of which some tens to hundreds of thousands with heights of hundreds of metres or taller are estimated to exist (25; 26). Thus, in this work, we combine the latest developments in our theoretical understanding of wake generation with a state-of-the-art global seamount census, to perform a baseline assessment of the role of topographic wakes in sustaining deep-ocean mixing and upwelling. This allows us to address the fundamental question originally posed by Munk & Wunsch (8): "Are seamounts and islands the stirring rods of the oceans?"

Global Seamount Census

Our analysis is founded on the seamount dataset of Kim & Wessel (27, hereafter KW11), which includes ∼25,000 seamounts with heights in excess of 100 m in areas away from continental margins. Approximately 8,500 of these seamounts are taller than 1 km. Those authors predict that their database likely underestimates the global inventory of seamounts by nearly a factor of two, such that the total number of seamounts may lie in the 40,000–55,000 range. Thus, the KW11 database is conservative, as it includes a significantly lower number of seamounts than earlier predictions. For example, Wessel *et al.*(25) reported more than 100,000 seamounts with heights exceeding 1 km, and speculated that there are probably 25 million seamounts taller than 100 m. Similarly, Yesson *et al.*(26) reported ∼140,000 seamounts with peak heights between 500 m and 1 km, and ∼ 33,500 seamounts taller than 1 km. The KW11 data incorporates corrections for the ambiguity in gravity signals due to small seamounts and for the overlap with abyssal hills. As a result, seamounts captured by the KW11 data are distinct from abyssal hills, and correspond instead to active or extinct undersea volcanoes with heights in excess of 100 m. It is worth noting that in the three realistic simulations used in this study, each using high resolution bathymetry derived from multi-beam surveys, there are multiple examples of seamounts that are not found in the KW11 seamount census, emphasizing the conservative seamount count of KW11. Figure 1b shows the global distribution of the KW11 seamounts, coloured by their height. For reference, the local depth is shown in panel a.

Flow Around a Seamount

A flow past a seamount generates a turbulent topographic wake with patches of both cyclonic and anticyclonic vorticity, leading to instabilities and formation of SCVs with either sign of vorticity in the wake of the seamount (23; 24; 28; 29). While two-dimensional (2D) wake flow past a cylinder is a classic focal problem in fluid mechanics, the description of 3D seamount wakes in a rotating density-stratified ocean is a recently-attacked, and far more complicated, problem. The impacts on wake dynamics of rotation and stratification can be encapsulated in two dimensionless numbers: the Rossby number $Ro = \frac{U}{fD}$, and the Froude number $Fr = \frac{U}{NH}$, where U is the horizontal velocity, f is the Coriolis frequency, N is the buoyancy frequency, H is the height of the seamount, and D is the diameter of the seamount at its mid-height. The Froude number gives the ratio of the energetically possible amplitude of vertical fluid displacement to the seamount height. A small Froude number ($Fr < 1$) implies that the flow skirts seamounts and leads predominantly to the generation of wake vortices, with potentially some lee wave generation at the top (Fig. 1d); in contrast, a large Froude number ($Fr > 1$) describes a regime with a substantial flow component directed over the seamount, resulting in a stronger radiation of topographic lee waves in addition to the wake. We note that there exists an extensive literature on flow over mountains in the atmospheric context, but such flows often correspond to higher Froude numbers as compared to the oceanic flows over seamounts and thus the dynamics are dominated by lee wave generation which is not our focus herein (30; 31).

The vertical structure of wake vortices has been found to further depend on the Rossby and Froude numbers too or, specifically, on their ratio, which is expressed by the Burger number $Bu = (Ro/Fr)^2 = (\frac{NH}{fD})^2$. The Burger number can also be viewed as the (squared) ratio of an effective Rossby deformation radius $R_D \sim NH/f$, (where the seamount height H replaces the ocean depth as the relevant vertical lengthscale), and the mid-height seamount diameter D. Small Bu values are associated with vertically coherent vortices (with horizontal scale set by the deformation radius), whereas large Bu values characterize layered vortices (with horizontal scale

at a given depth set by the local seamount diameter at that height) (23) – see Fig. 1d. This latter case carries important implications for the generation of small-scale turbulence within the wakes, due to the strong vertical shear between the vortices' layers (24; 32). Thus, equatorial topographic wakes may be expected to be particularly effective at generating small-scale turbulence, as the equatorward-decreasing f results in more vertically-sheared wake structures and elevated turbulent energy dissipation (33). The dependence on Bu of dynamical regimes of flow impingement on seamounts outlined here has been recently explored and corroborated with large eddy simulations (32; 34).

In this work, we set aside the lee wave radiation regime (Fig. 1d) which, despite its regional significance, has been investigated within earlier studies of lee wave generation over generalized rough topography (35; 36). We also exclude the influence of tides as we find that the tidal excursion is generally small compared to the horizontal scale of the seamounts, and the tidal flows are thus likely to be secondary to the mean flow in the generation of wake vortices (see Supplementary Information). However, tidal interaction with seamounts may also be important for enhancing mixing (37; 38). Instead, our focus will be on the turbulent mixing induced by vertically-sheared, layered vortices forming in the wake of seamounts across the world ocean. To our knowledge, the basin-scale impacts of this regime of flow-seamount interaction have not been considered to date, yet, as we will see, such impacts are predicted to be of considerable importance to the global ocean circulation.

In Figure 1c, we construct a map of Fr based on the KW11 seamount data and climatological stratification (WOCE; 39), and a field of root-mean-square flow speed (at the mid-depths of the KW11 seamounts) calculated from a $1/48^\circ$ resolution ocean model simulation, initiated by the Estimating the Circulation and Climate of the Ocean (ECCO) project, and hence observationally-constrained (40, see Supplementary Materials). The dependence of Fr on flow speed highlights regions known to be associated with intense flows such as the Antarctic Circumpolar Current (ACC) system, western boundary currents, abyssal channels and passages, etc. The corresponding estimate of Bu is displayed in Figure 1e, illustrating that, overall, seamount wakes are expected to be more layered around the equator due to the inverse dependence of Bu on f. At high latitudes (*e.g.*, in the ACC region) flow impingement on seamounts is instead mostly predicted to generate barotropic vortices. Note however that substantial regional departures from this general pattern do occur, linked primarily to the seamount aspect ratio H/D.

A basin-by-basin histogram synthesis of the height-to-local-depth ratio and Bu of the seamount field is provided by Figure 1f. The Pacific Ocean stands out in that it hosts larger percentages of high-Bu and tall (relative to the local depth) seamounts than other basins. The more frequent occurrence of high-Bu regimes makes the Pacific Ocean particularly favourable to the development of shear-induced turbulence associated with layered wake vortices. In contrast, the Southern Ocean seamounts are expected to mostly produce barotropic vortices, with the Atlantic and Indian basins falling in between the Pacific and Southern Ocean extremes. The Pacific Ocean's comparative richness of 'locally tall' seamounts further suggests that seamount-induced dynamics in this basin may impact shallower waters than in the rest of the world ocean.

Based on idealized numerical simulations of flow around isolated seamounts, Perfect *et al.* (32) reported that the volume-averaged turbulent diapycnal diffusivity follows the scaling

$$K \sim (Fr\, Ro)^2. \tag{1}$$

This vortex-associated diffusivity may exceed background turbulent levels in the ocean interior ($K \sim 10^{-5}$ $\mathrm{m^2 s^{-1}}$) for $Fr\, Ro \geq 0.005$, and can be as large as mixing rates in the most energetic tidal zones ($K \geq 10^{-3}$ $\mathrm{m^2 s^{-1}}$). The scaling of Eq. 1 exhibits qualitative consistency with the recent results of Srinivasan *et al.*(33). Next, we will show that the preceding theoretical framework, which was developed within highly idealized scenarios (32), provides an adequate characterization of flow impingement on a field of seamounts. We will do this through the analysis of three high-resolution realistic models of the ocean circulation in three paradigmatic regions: an equatorial area (representing the large-Bu limit with strongly-sheared, layered topographic vortices); a patch of the Southern Ocean (indicative of the small-Bu limit dominated by barotropic vortices and lee waves); and the intermediate case of a mid-latitude, seamount-rich area around the New England Seamount Rise. Having demonstrated the theory's applicability in these realistic settings, we will then apply the scaling relation for the diapycnal diffusivity introduced above to the KW11 seamount data (Fig. 1b) and climatological stratification and flow speed data (Fig. 1c) to assess the contribution of seamount-induced mixing to deep-ocean upwelling on a global scale.

Equatorial Seamounts: an Example of Layered Vortices

The validity of the theoretical description of flow around a seamount in a realistic high-Bu setting is illustrated with a regional simulation in the equatorial Atlantic Ocean (Fig. 2; see Supplementary Materials for a detailed description of the simulation). Snapshots of relative vorticity at a vertical level (2800 m) intersected by seamounts (Fig. 2a) and along a vertical section crossing the model domain (Fig. 2b) reveal the occurrence of intense cyclonic and anticyclonic filaments and vortices in the wake of the seamounts, following a predominantly

south-Eastward current below 1500 m. These features exhibit complex, vertically layered structures that are associated with intense vertical shears (Fig. 2e), and are thus expected to generate strong turbulent mixing. That the simulated wake vortices conform to theoretical predictions may be illustrated by estimating the set of dimensionless parameters on which the theory is founded. The modelled flows around the seamounts are characterized by a typical Rossby number $Ro \sim 1$, a Froude number $Fr \sim 0.01 - 0.1$, and a Burger number $Bu \sim 100 - 10,000$. These correspond squarely to the layered wake vortex regime (Fig. 1d), and thereby indicate that the area should have a rich field of layered topographic vortices (33) – as indeed it is found to do.

The simulation further lends support to the scaling relation for the diapycnal diffusivity produced by idealized numerical experiments (Eq. 1). Specifically, the vertically sheared layers in the simulation give rise to critical Richardson number values that, in turn, yield high diffusivities of as much as $O(10^{-3} - 10^{-2})$ in the wakes of seamounts (Figs. 2f,g). These diffusivities exceed those away from topography by typically one to two orders of magnitude below 1500 m depth (Fig. 2d), and are in the range of (though, on average, slightly larger than) diffusivities predicted by the theoretical scaling (Fig. 2c). A comprehensive comparison of modelled and predicted diffusivities is provided in the Supplementary Materials.

Drake Passage: an Example of Barotropic Vortices

The Southern Ocean primarily hosts seamounts with $Bu < 1$ (Figs. 1e-f). As the deep-reaching jets and eddies of the ACC impinge on the Drake Passage seamounts, they are expected to generate barotropic wake vortices and lee waves. This prediction is tested here with a dynamically-downscaled regional simulation (Fig. 3a,b), based on the observationally forced and verified model of Mashayek *et al.*(41), but integrated at greatly refined vertical resolution to resolve the vertical mixing (as verified through comparison with observed mixing rates in Fig. 3c). A full description of the simulation is provided in the Supplementary Materials.

In contrast to the equatorial case study, the very rough topography of the Drake Passage consists of many less well-defined seamounts, some of which merge into ridges and larger-scale bathymetric features. This is readily apparent in Fig. 3b, where a chain of seamounts rising above a depth of 3000 m is seen to criss-cross the southeastern part of the simulation domain. The ACC's impingement on these seamounts leads to complex wake vortices (see map of relative vorticity at 3000 m in Fig. 3e) that interact non-linearly with one another as well as with their (larger-scale) parent mesoscale structures and (smaller-scale) lee waves. These same features are visible in a vertical section of relative vorticity (Fig. 3d), which additionally reveals that the topographic vortices are vertically extensive (*i.e.*, quasi-barotropic), as indicated by theory. Horizontal (Fig. 3g) and vertical (Fig. 3f) views of the diapycnal diffusivity in the model confirm that turbulent mixing is systematically enhanced around the topographic vortices (Fig. 3d,e), with diffusivity values approaching and exceeding $O(10^{-3})$ $\mathrm{m^2 s^{-1}}$ near the seafloor. It is not expected that the scaling (1) will be relevant in this scenario, as the mixing near topography is primarily due to breaking internal waves generated by the flow-topography interaction.

New England Seamounts: an Example of Mixed Dynamics

Intermediate cases with moderate Bu can also lead to intense mixing. For example, numerical simulations of the New England seamounts – a chain of deep seamounts on the path of the Gulf Stream – highlight the occurrence of intense turbulent wakes and high amplitude lee waves in the lee of the seamounts (Figs. 4a,b). These wakes can extend horizontally up to 100 km downstream, and vertically from the bottom to slightly above the peak of the seamounts.

The seamount shown in Fig. 4d has a shape similar to that of the idealized seamount studied by Perfect *et al.* (32), with characteristic values of $D = 25$ km for the half-width, $H = 3000$ m for the height, and a water depth of 5000 m. Locally, the Coriolis parameter is $f \sim 0.8 \times 10^{-4}\,\mathrm{s^{-1}}$, and the mean stratification is $N \sim 1 \times 10^{-3}\,\mathrm{s^{-1}}$, corresponding to a typical Rossby number $Ro \sim 0.1$, a Froude number $Fr \sim 0.1$, and a Burger number $Bu \sim 2$. The vortical wake structure is thus expected to be more vertically coherent than in the equatorial case, as confirmed by the simulation (Fig. 4b and supplementary animation).

The vortical wake is associated with an enhancement of turbulent mixing, again by one to two orders of magnitude relative to typical levels at the same depth away from the seamounts (Fig. 4d). In this case, the elevated diffusivities are localized predominantly on the anticyclonic side of the wake, as is characteristic of centrifugal instability in the near wake for extratropical cases with $Ro < 1$ (33). The diffusivities exceed again those predicted by the theoretical scaling (Fig. 4c), as further described in the Supplementary Materials.

Global Deep-Ocean Mixing and Upwelling

Next, we explore the global implications of seamount induced mixing by applying Eq. (1) to the KW11 dataset and climatological hydrographic data (WOCE). Specifically, we *only* account for the turbulence induced by the shear in between the layered wake vortices ($Bu > 1$), which is absent from representation of ocean turbulence

in climate models (and hence is the novelty of this work), and not the mixing associated with seamount-radiated internal lee waves or wave-vortex interactions which can have overlaps with existing mixing estimates. The outcome is shown in Fig. 5a –the details of the map's construction are discussed in the Supplementary Materials. For comparison, panels c and d respectively display the diffusivities associated with internal tides and lee waves on an illustrative deep-ocean density level. Seamount-generated mixing is found to be intense compared to the most energetic tidal and lee wave mixing, specially at lower latitudes, although strong tidal mixing is substantially more widely spread. The map in panel a is entirely absent from mixing parameterizations in ocean and climate general circulation models. Our decision to exclude the tidal or lee wave mixing induced by seamounts ensures that there is no overlap between panels a and c,d.

The impact on deep-ocean upwelling of seamount-generated mixing is assessed by quantifying the rate of water mass transformation effected by this and other (*i.e.*, internal tides and lee waves) mixing agents. The characteristic distribution of the diapycnal velocity induced by the three mixing agents considered may be illustrated with an example from a deep isopycnal in the Pacific Ocean (Fig. 5e), where red and blue respectively denote local lightening (*i.e.*, diapycnal upwelling) and densification (*i.e.*, diapycnal downwelling)– see Supplementary Materials for a description of the calculation. As found by other recent works (42; 2; 43; 44), downwelling is prevalent in the interior of basins, but intense upwelling occurs near topographic boundaries, where the selected isopycnal approaches the seafloor. When integrated globally (Fig. 5f) or across the Pacific (Fig. 5h), as much as tens of Sverdrups (1 Sv $\equiv 10^{-6}$ m^3 s^{-1}) of deep waters down- or upwell across isopycnals, leading to a smaller residual net (*i.e.*, upwelling minus downwelling) diapycnal transfer on the order of 1-10 Sv for all deep-ocean density classes (Figs. 5g,i).

Examination of the individual contributions of seamount-, internal tide- and lee wave-generated turbulence to the water mass transformation rate reveals that seamount-induced mixing is a leading-order player in both the upwelling and downwelling components of the transformation (Figs. 5f,h), as well as in the net global- or basin-scale diapycnal transfers (Figs. 5g,i). For most deep density classes, seamount-generated mixing contributes O(30%) or larger of the tidal upwelling, downwelling or residual transformation; tidal component is of course expected to be dominant (35; 44).

We emphasize that our estimates are conservative due to four factors: (I) the seamount count of KW11 is likely very conservative; for example all three of our regional examples included many seamounts missing from KW11, (II) we only accounted for high Bu tall seamounts (e.g., compare Fig 5a with Fig 1b); other seamounts also contribute to mixing, (III) we only accounted for shear-induced turbulence in between layered vortical wakes; seamounts generate mixing due to wave generation, wave-vortex interactions, near boundary instabilities, and tide-seamount interactions, none of which were accounted for here, and (IV) the formula used to infer mixing from the seamount dataset seems to underpredict mixing compared to our regional high-resolution model outputs.

Discussion

We have demonstrated that theoretical descriptions of the turbulent mixing generated by flow impingement on seamounts, which were developed for highly idealized scenarios, hold broadly for realistic flow and topography configurations. By conservatively applying these theoretical ideas to global seamount and oceanographic datasets, we have shown that turbulence associated with seamount-generated layered vortices makes a leading-order contribution to deep-ocean mixing and upwelling – comparable to contributions from other, much more extensively studied sources of turbulence. We conclude that seamount-induced turbulence may be a significant, hitherto-overlooked new player in the ongoing debate around the closure of the overturning circulation's deep upwelling limb (45; 46; 47; 48; 49; 50; 51; 52; 53). This appears particularly plausible near the equator and in the subtropics, where the layered vortex regime highlighted in our work occurs widely.

Despite this regime's likely important role in shaping the deep ocean circulation, there have been, to our knowledge, no observations of seamount-generated layered vortices and their associated mixing to date. As such, the mixing effects of seamounts are absent from state-of-the-art climate-scale ocean models. Furthermore, one of the largest uncertainties in the estimates presented here is the potentially significant underestimate in the number of seamounts in the KW11 dataset, thus future improvements to global bathymetric maps will also play an important role in quantifying seamount driven mixing. We suggest that addressing these major knowledge gaps will require not only first-of-their-kind observations and model parameterizations of seamount-generated turbulence, but also advances in dynamical understanding of the evolution of the separated vortices. This evolution may implicate a variety of instabilities (19; 17; 24; 33), and interactions with both submesoscale phenomena at the bottom boundary (13; 14; 15; 16), seamount-radiated lee waves (34), and near-inertial waves (22). The ground is thus laid for the ocean mixing community to drive a fruitful, multi-faceted expansion of this new area of research.

Acknowledgments

The data used to produce figures 1 and 5, along with the scripts used for the analyses, will be made available upon acceptance of this article. Data from simulations described in figures 2,3 and 4 will be available from Ali Mashayek and Jonathan Gula upon request.

References

[1] C. De Lavergne, G. Madec, J. Le Sommer, A. G. Nurser, and A. C. Naveira Garabato, "On the consumption of antarctic bottom water in the abyssal ocean," *Journal of Physical Oceanography*, vol. 46, no. 2, pp. 635–661, 2016.

[2] R. Ferrari, A. Mashayek, T. J. McDougall, M. Nikurashin, and J.-M. Campin, "Turning ocean mixing upside down," *Journal of Physical Oceanography*, vol. 46, no. 7, pp. 2239–2261, 2016.

[3] S. E. M. Fletcher, N. Gruber, A. R. Jacobson, S. C. Doney, S. Dutkiewicz, M. Gerber, M. Follows, F. Joos, K. Lindsay, D. Menemenlis, A. Mouchet, S. A. Müller, and J. L. Sarmiento, "Inverse estimates of anthropogenic CO_2 uptake, transport, and storage by the ocean," *Global Biogeochem. Cyc.*, vol. 20, no. 2, p. doi:10.1029/2005GB002530, 2006.

[4] A. J. Watson, G. K. Vallis, and M. Nikurashin, "Southern ocean buoyancy forcing of ocean ventilation and glacial atmospheric CO_2," *Nature Geosci.*, vol. 8, pp. 861–864, 2015.

[5] M. Nikurashin and G. K. Vallis, "A theory of the interhemispheric meridional overturning circulation and associated stratification," *J. Phys. Oceanogr.*, vol. 42, pp. 1652–1667, 2012.

[6] A. F. Thompson, A. Stewart, and T. Bischoff, "A multi-basin residual-mean model for the global overturning circulation," *J. Phys. Oceanogr.*, vol. 46, pp. 2583–2602, 2016.

[7] H. F. Drake, R. Ferrari, and J. Callies, "Abyssal circulation driven by near-boundary mixing: watermass transformations and interior stratification," *J. Phys. Oceanogr.*, vol. 50, pp. 2203–2226, 2020.

[8] W. Munk and C. Wunsch, "Abyssal recipes II: energetics of tidal and wind mixing," *Deep-Sea Research*, vol. 45, pp. 1977–2010, 1998.

[9] C. B. Whalen, C. de Lavergne, A. C. Naveira Garabato, J. M. Klymak, J. A. MacKinnon, and K. L. Sheen, "Internal wave-driven mixing: governing processes and consequences for climate," *Nature Reviews Earth & Environment*, vol. 1, no. 11, pp. 606–621, 2020.

[10] K. L. Polzin and T. J. McDougall, "Mixing at the ocean's bottom boundary," *Ocean Mixing: Drivers, Mechanisms and Impacts*, pp. 145–180, 2021.

[11] M. H. Alford, J. B. Girton, G. Voet, G. S. Carter, J. B. Mickett, and J. M. Klymak, "Turbulent mixing and hydraulic control of abyssal water in the samoan passage," *Geophys. Res. Lett.*, vol. 40, pp. 4668–4674, 2013.

[12] L. Clément and A. M. Thurnherr, "Abyssal upwelling in mid-ocean ridge fracture zones," *Geophysical Research Letters*, vol. 45, no. 5, pp. 2424–2432, 2018.

[13] J. O. Wenegrat, J. Callies, and L. N. Thomas, "Submesoscale baroclinic instability in the bottom boundary layer," *Journal of Physical Oceanography*, vol. 48, no. 11, pp. 2571–2592, 2018.

[14] A. C. Naveira Garabato, E. E. Frajka-Williams, C. P. Spingys, S. Legg, K. L. Polzin, A. Forryan, E. P. Abrahamsen, C. E. Buckingham, S. M. Griffies, S. D. McPhail, K. W. Nicholls, L. N. Thomas, and M. P. Meredith, "Rapid mixing and exchange of deep-ocean waters in an abyssal boundary current," *Proceedings of the National Academy of Sciences*, vol. 116, no. 27, pp. 13233–13238, 2019.

[15] J. O. Wenegrat and L. N. Thomas, "Centrifugal and symmetric instability during ekman adjustment of the bottom boundary layer," *Journal of Physical Oceanography*, vol. 0, no. 0, p. null, 2020.

[16] J. Gula, J. Taylor, A. Shcherbina, and A. Mahadevan, *Ocean Mixing: Drivers, Mechanisms and Impacts*, ch. Submesoscale processes and Mixing, pp. 181–214. Elsevier BV, 2022.

[17] J. Gula, M. Molemaker, and J. C. McWilliams, "Topographic generation of submesoscale centrifugal instability and energy dissipation," *Nat. Commu.*, vol. 7, p. 12811, 2016.

[18] J. C. McWilliams, "Submesoscale currents in the ocean," *Proc. R. Soc. A*, vol. 472, no. 2189, 2016.

[19] M. Molemaker, J. C. McWilliams, and W. Dewar, "Submesoscale instability and generation of mesoscale anticyclones near a separation of the California Undercurrent," *J. Phys. Oceanogr.*, vol. 45, pp. 613–629, 2015.

[20] C. Vic, G. Roullet, X. Carton, X. Capet, M. Molemaker, and J. Gula, "Eddy-topography interactions and the fate of the Persian Gulf Outflow," *J. Geophys. Res. Oceans*, vol. 120, p. 6700–6717, 2015.

[21] W. Dewar, M. Molemaker, and J. C. McWilliams, "Centrifugal instability and mixing in the California Undercurrent," *J. Phys. Oceanogr.*, vol. 45, pp. 1224–1241, 2015.

[22] T. Nagai, D. Hasegawa, E. Tsutsumi, H. Nakamura, A. Nishina, T. Senjyu, T. Endoh, T. Matsuno, R. Inoue, and A. Tandon, "The kuroshio flowing over seamounts and associated submesoscale flows drive 100-km-wide 100-1000-fold enhancement of turbulence," *Communications Earth & Environment*, vol. 2, no. 1, p. 170, 2021.

[23] B. Perfect, N. Kumar, and J. J. Riley, "Vortex structures in the wake of an idealized seamount in rotating, stratified flow," *Geophysical Research Letters*, vol. 45, no. 17, pp. 9098–9105, 2018.

[24] K. Srinivasan, J. C. McWilliams, M. J. Molemaker, and R. Barkan, "Submesoscale vortical wakes in the lee of topography," *Journal of Physical Oceanography*, vol. 49, no. 7, pp. 1949–1971, 2019.

[25] P. Wessel, D. T. Sandwell, and S.-S. Kim, "The global seamount census," *Oceanography*, vol. 23, no. 1, pp. 24–33, 2010.

[26] C. Yesson, M. R. Clark, M. L. Taylor, and A. D. Rogers, "The global distribution of seamounts based on 30 arc seconds bathymetry data," *Deep Sea Research Part I: Oceanographic Research Papers*, vol. 58, no. 4, pp. 442–453, 2011.

[27] S.-S. Kim and P. Wessel, "New global seamount census from altimetry-derived gravity data," *Geophysical Journal International*, vol. 186, no. 2, pp. 615–631, 2011.

[28] J. Gula, T. M. Blacic, and R. E. Todd, "Submesoscale coherent vortices in the Gulf Stream," *Geophys. Res. Lett.*, vol. 46, 2019.

[29] D. C. Napolitano, I. C. A. da Silveira, A. Tandon, and P. H. R. Calil, "Submesoscale phenomena due to the brazil current crossing of the vitória-trindade ridge," *Journal of Geophysical Research: Oceans*, vol. 126, no. 1, p. e2020JC016731, 2021. e2020JC016731 2020JC016731.

[30] M. Wurtele, R. Sharman, and A. Datta, "Atmospheric lee waves," *Annual review of fluid mechanics*, vol. 28, no. 1, pp. 429–476, 1996.

[31] R. B. Smith, "100 years of progress on mountain meteorology research," *Meteorological Monographs*, vol. 59, pp. 20–1, 2019.

[32] B. Perfect, N. Kumar, and J. J. Riley, "Energetics of seamount wakes. part i: Energy exchange," *Journal of Physical Oceanography*, vol. 50, no. 5, pp. 1365–1382, 2020.

[33] K. Srinivasan, J. C. McWilliams, and A. Jagannathan, "High vertical shear and dissipation in equatorial topographic wakes," *Journal of Physical Oceanography*, 2021.

[34] B. Perfect, N. Kumar, and J. J. Riley, "Energetics of seamount wakes. part ii: Wave fluxes," *Journal of Physical Oceanography*, vol. 50, no. 5, pp. 1383–1398, 2020.

[35] M. Nikurashin and R. Ferrari, "Overturning circulation driven by breaking internal waves in the deep ocean," *Geophysical Research Letters*, vol. 40, no. 12, pp. 3133–3137, 2013.

[36] A. C. N. Garabato, A. J. G. Nurser, R. B. Scott, and J. A. Goff, "The impact of small-scale topography on the dynamical balance of the ocean," *J. Phys. Oceanogr.*, vol. 43, pp. 647–668, 2013.

[37] E. Kunze and J. M. Toole, "Tidally driven vorticity, diurnal shear, and turbulence atop fieberling seamount," *Journal of Physical Oceanography*, vol. 27, no. 12, pp. 2663–2693, 1997.

[38] P. Puthan, S. Sarkar, and G. Pawlak, "Tidal synchronization of lee vortices in geophysical wakes," *Geophysical Research Letters*, vol. 48, no. 4, p. e2020GL090905, 2021.

[39] V. Gouretski and K. P. Koltermann, "WOCE global hydrographic climatology," *Berichte des BSH*, vol. 35, pp. 1–52, 2004.

[40] B. K. Arbic, M. H. Alford, J. K. Ansong, M. C. Buijsman, R. B. Ciotti, J. T. Farrar, R. W. Hallberg, C. E. Henze, C. N. Hill, C. A. Luecke, *et al.*, "Primer on global internal tide and internal gravity wave continuum modeling in HYCOM and MITgcm," *New frontiers in operational oceanography*, pp. 307–392, 2018.

[41] A. Mashayek, R. Ferrari, S. Merrifield, J. R. Ledwell, L. St Laurent, and A. N. Garabato, "Topographic enhancement of vertical turbulent mixing in the Southern Ocean," *Nature communications*, vol. 8, p. 14197, 2017.

[42] C. de Lavergne, G. Madec, J. Le Sommer, A. J. G. Nurser, and A. C. Naveira Garabato, "On the Consumption of Antarctic Bottom Water in the Abyssal Ocean," *Journal of Physical Oceanography*, vol. 46, pp. 635–661, 2 2016.

[43] A. Mashayek, H. Salehipour, D. Bouffard, C. P. Caulfield, R. Ferrari, M. Nikurashin, W. R. Peltier, and W. D. Smyth, "Efficiency of turbulent mixing in the abyssal ocean circulation," *Geophysical Research Letters*, vol. 44, no. 12, pp. 6296–6306, 2017.

[44] L. Cimoli, C. P. Caulfield, H. L. Johnson, D. P. Marshall, A. Mashayek, A. C. Naveira Garabato, and C. Vic, "Sensitivity of Deep Ocean Mixing to Local Internal Tide Breaking and Mixing Efficiency," *Geophysical Research Letters*, vol. 46, pp. 14622–14633, 12 2019.

[45] W. H. Munk and C. Wunsch, "Abyssal recipes II: Energetics of tidal and wind mixing," *Deep-Sea Research*, vol. 45, pp. 1977–2010, 1998.

[46] L. D. Talley, J. L. Reid, and P. E. Robbins, "Data-based meridional overturning streamfunctions for the global ocean," *Journal of Climate*, vol. 16, no. 19, pp. 3213–3226, 2003.

[47] C. Wunsch and R. Ferrari, "Vertical mixing, energy, and the general circulation of the oceans," *Annu. Rev. Fluid Mech.*, vol. 36, pp. 281–314, 2004.

[48] R. Lumpkin and K. Speer, "Global ocean meridional overturning," *Journal of Physical Oceanography*, vol. 37, no. 10, pp. 2550–2562, 2007.

[49] L. Talley, "Closure of the Global Overturning Circulation Through the Indian, Pacific, and Southern Oceans: Schematics and Transports," *Oceanography*, vol. 26, pp. 80–97, 3 2013.

[50] A. F. Waterhouse, J. A. MacKinnon, J. D. Nash, M. H. Alford, E. Kunze, H. L. Simmons, K. L. Polzin, L. C. St. Laurent, O. M. Sun, R. Pinkel, and others, "Global patterns of diapycnal mixing from measurements of the turbulent dissipation rate," *Journal of Physical Oceanography*, vol. 44, no. 7, pp. 1854–1872, 2014.

[51] R. Ferrari, "Oceanography: What goes down must come up," *Nature*, vol. 513, no. 7517, pp. 179–180, 2014.

[52] T. Huussen, A. Naveira-Garabato, H. Bryden, and E. McDonagh, "Is the deep indian ocean MOC sustained by breaking internal waves?," *Journal of Geophysical Research: Oceans*, vol. 117, 2012.

[53] L. Cimoli *et al.*, "Significance of diapycnal mixing within the Atlantic Meridional Overturning Circulation," *Nature Communications*, 2021.

[54] C. de Lavergne, C. Vic, G. Madec, F. Roquet, A. F. Waterhouse, C. Whalen, Y. Cuypers, P. Bouruet-Aubertot, B. Ferron, and T. Hibiya, "A parameterization of local and remote tidal mixing," *Journal of Advances in Modeling Earth Systems*, vol. 12, no. 5, p. e2020MS002065, 2020.

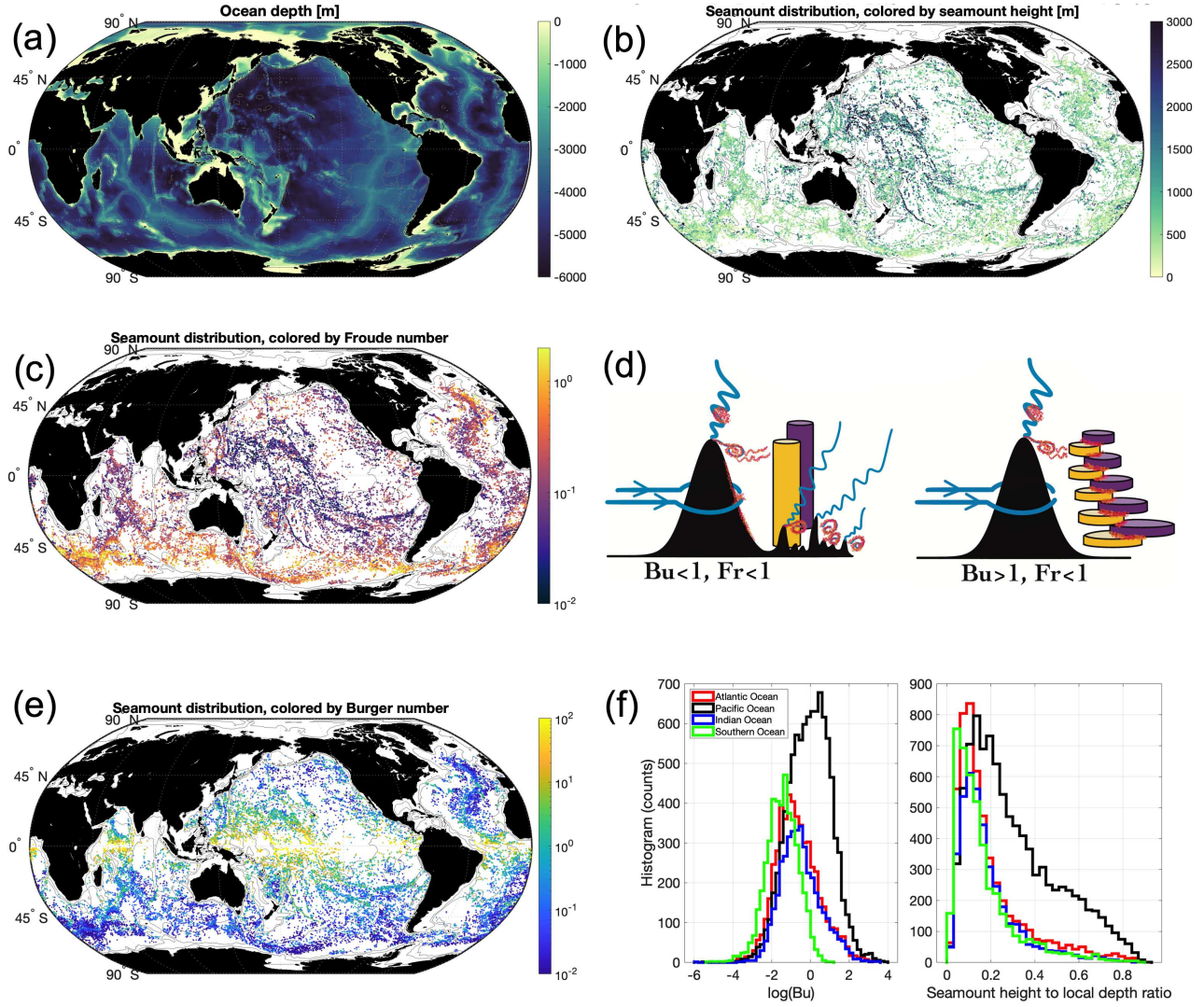

Figure 1: (a) Ocean depth. (b) Global distribution of seamounts (from (27)), composed of ∼25,000 seamounts, (c) Same as panel b, but coloured based on the seamount Froude number. (d) A schematic summarizing the various dynamical paradigms of flow around seamounts as a function of Burger and Froude numbers.(e) Same as panel b, but coloured based on the seamount Burger number. (f) Histogram of seamounts based on their Burger numbers and divided into different basins. A map of Froude number for the seamounts is included in the Supplementary Materials.

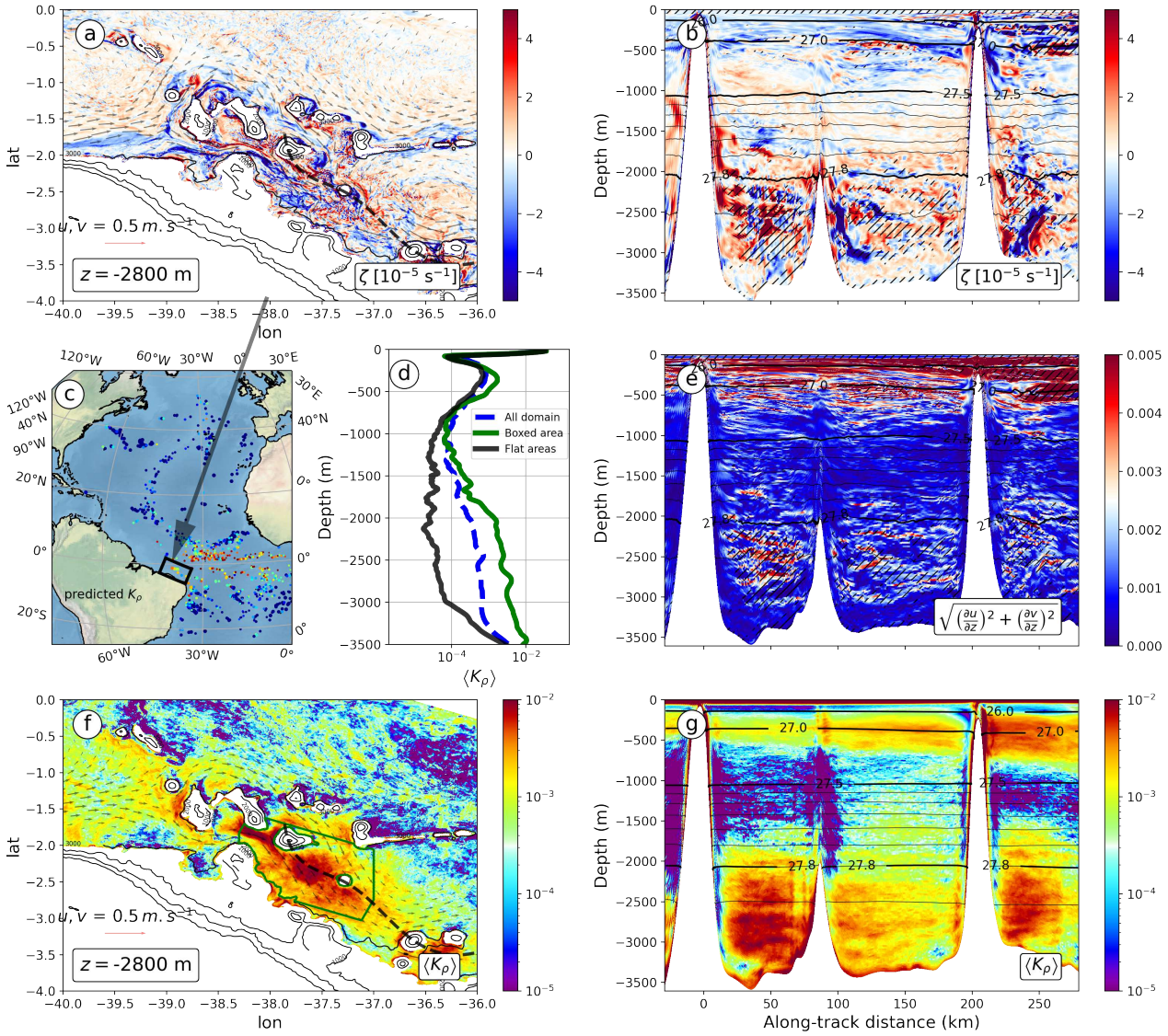

Figure 2: (a,b) Snapshots of relative vorticity (a) at 2800 m depth in the equatorial Atlantic Ocean, and (b) along an approximately along-stream vertical section crossing several seamounts (shown as a dashed line on panel a). Hatched regions highlight instantaneous vertical mixing coefficient K_ρ larger than 10^{-4}. (c) Predicted vertical mixing coefficient K_ρ from the seamount database. The simulation domain is shown in black. (d) Vertical profiles of K_ρ spatially integrated over the full simulation domain in blue, over the seamount region in green (see green domain in panel f), and over a region away from seamounts in black. (e) Snapshot of vertical velocity shear along the same along-stream vertical section than in (b). (f,g) Time-averaged vertical mixing coefficient K_ρ (f) at 2800 m depth, and (g) along the same along-stream vertical section than in (b,e).

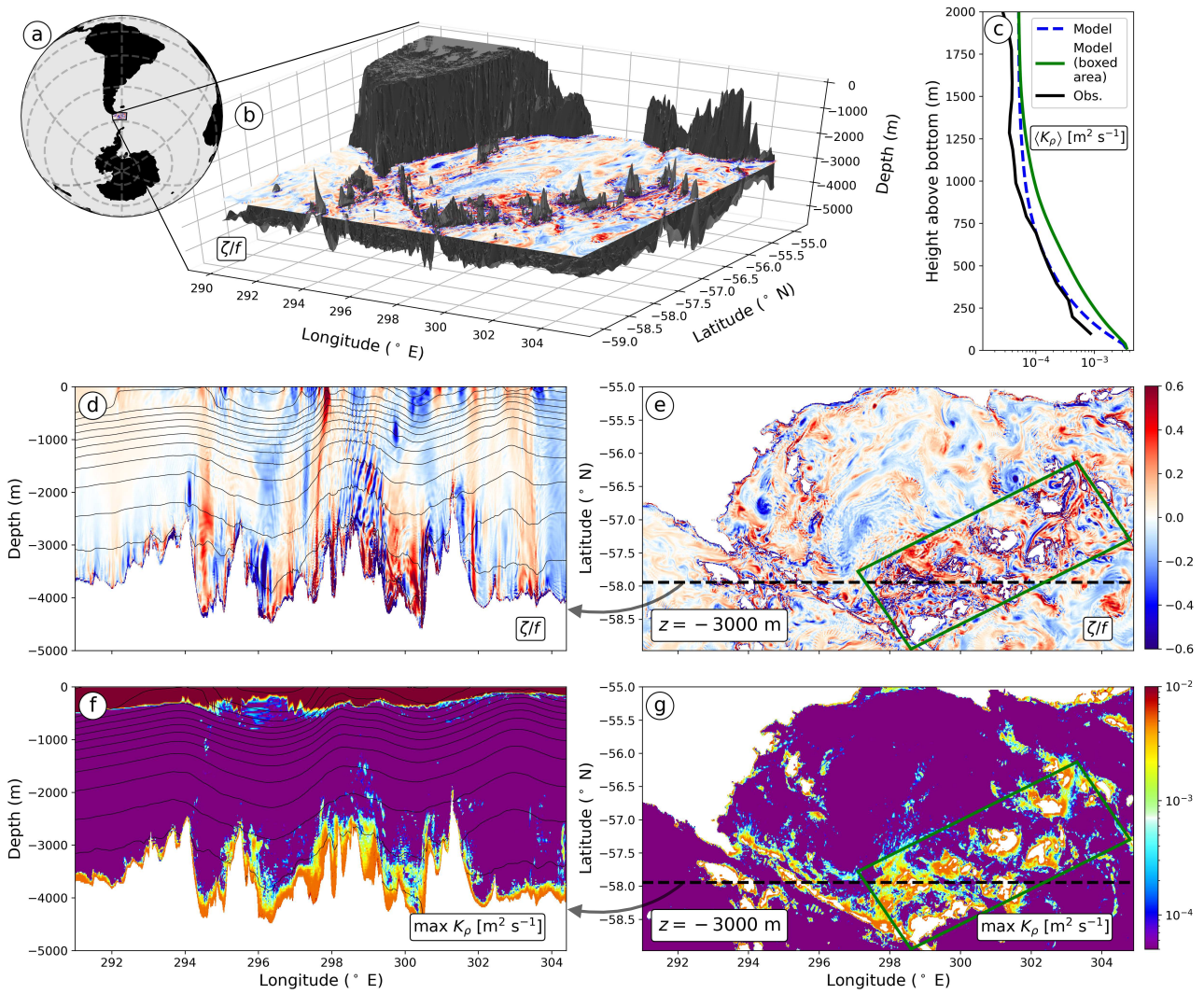

Figure 3: (a,b) The domain of the observationally forced and verified Drake Passage model, a full description of which is in the Supplementary Materials. The contour shows relative vorticity, ζ/f, at 3000m depth to illustrate the wake vortices flowing through the seamount ranges. (c) Model vertical diffusivity averaged over 20 days in the whole domain (blue dashed) and over the boxed region in panels e and g (green) and microstructure observations of diffusivity in the same box (black). (d) vertical section along dashed line in panel e. (e) top view of panel b. (f) 20-day maximum of the vertical mixing (diapycnal diffusivity) on the same slice as in panel d. (g) same as panel e but top view of a slice at 3000m depth.

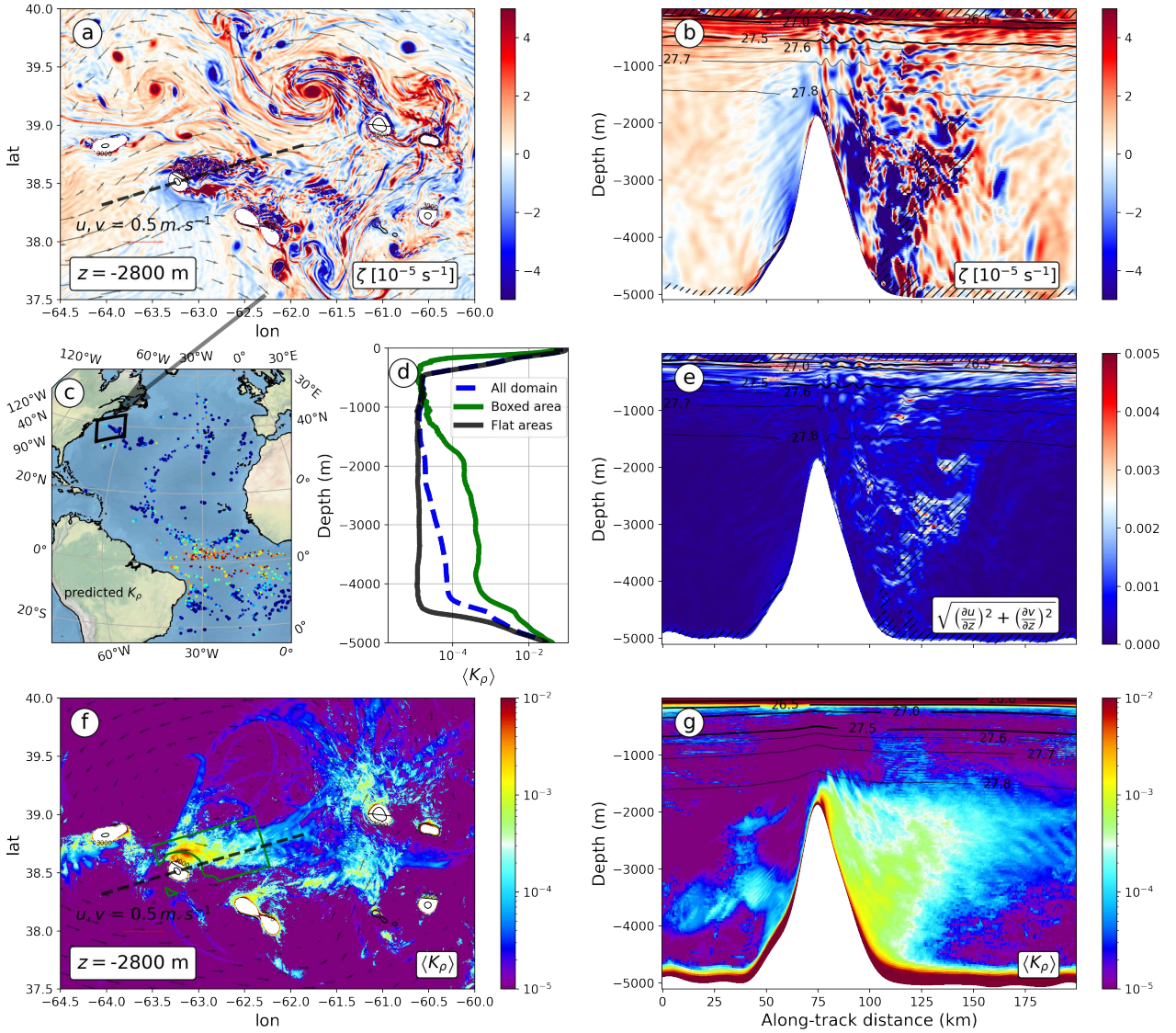

Figure 4: (a,b) Snapshots of relative vorticity (a) at 2800 m depth in the North Atlantic ocean, and (b) along an approximately along-stream vertical section crossing a seamount (shown as a dashed line on panel a). Hatched regions highlight instantaneous vertical mixing coefficient K_ρ larger than 10^{-4}. (c) Predicted vertical mixing coefficient K_ρ from the seamount database. The simulation domain is shown in black. (d) Vertical profiles of K_ρ spatially integrated over the full simulation domain in blue, over the seamount region in green (see green domain in panel f), and over a region away from seamounts in black. (e) Snapshot of vertical velocity shear along the same along-stream vertical section than in (b). (f,g) Time-averaged vertical mixing coefficient K_ρ (f) at 2800 m depth, and (g) along the same along-stream vertical section than in (b,e).

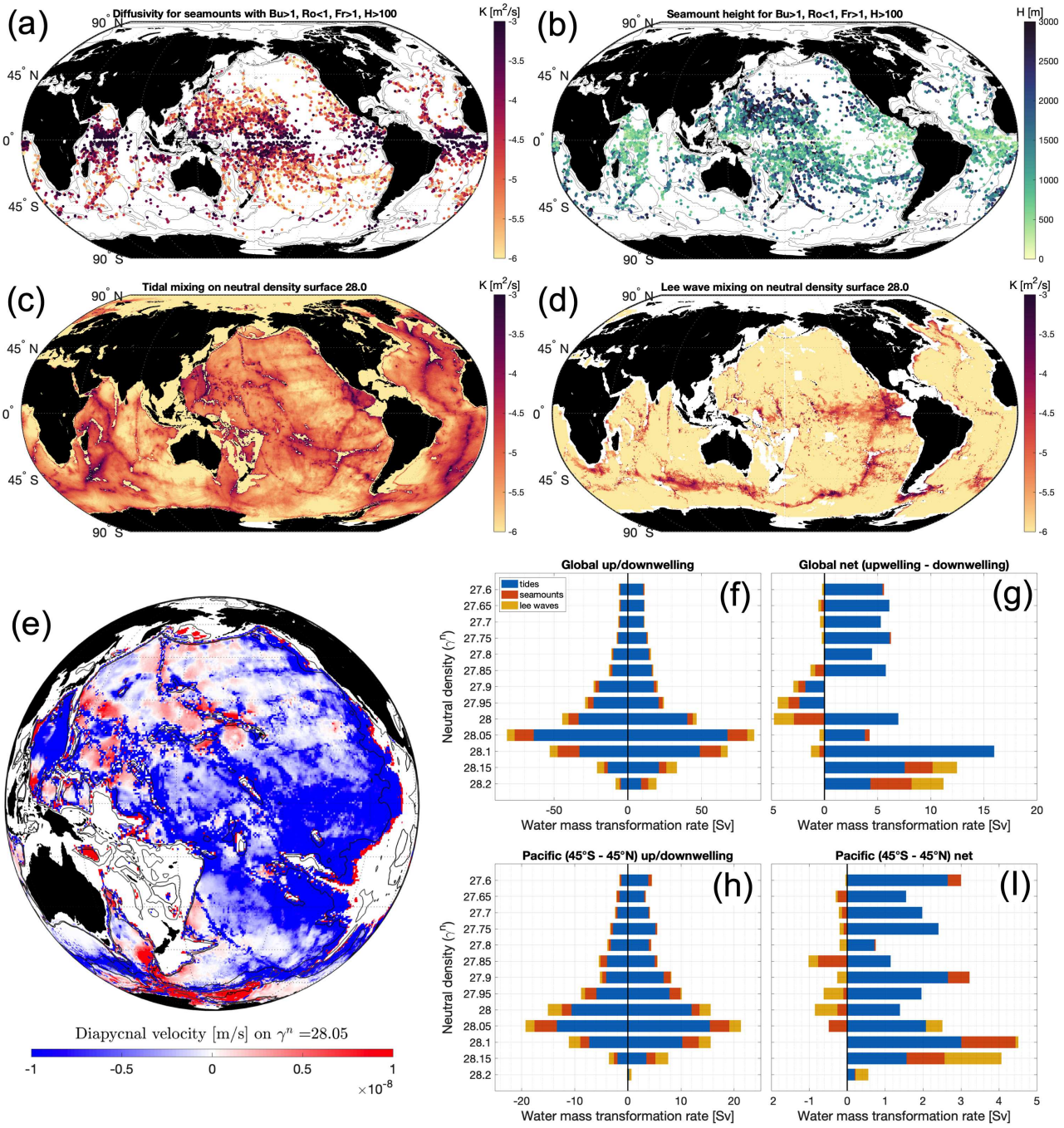

Figure 5: (a) Distribution of seamounts that are expected to give rise to shear-induced turbulence due to baroclinic vortex decoupling in their wakes ($Bu > 1$). Seamounts with $Ro > 1$ (too close to the equator and not accounted for in Eq. (1)), $Fr > 1$ (for which flow goes primarily above them rather than around them), and H<100m (fully or partially within the bottom turbulent boundary layer) are all discarded from the map shown in Figure 1. The colour coding implies the effective turbulent diffusivity that represents the mixing around and over the height of seamounts as per Eq. (1) (b) The corresponding seamount heights for the seamounts in panel a. (c) Turbulent diffusivity from tidal mixing on a deep density surface of 28 with a mean depth of 2000m and mean height above bottom of 2160m (from 54).(d) Turbulent diffusivity from lee wave mixing on the same density layer as in panel c (from 35). (e) Diapycnal velocity calculated from the contribution of internal tides and lee waves on the density surface $\gamma^n = 28.05$. Positive values (red) indicate diapycnal upwelling, and negative values (blue) indicate diapycnal downwelling. (f-i) Water mass transformation rate in the global ocean (f,g) and in the 45°S - 45°N Pacific Ocean (h,i). In each panel, the net water mass transformation is split into the contribution of (blue) internal tides, (red) seamounts and (yellow) lee waves. Panels (f,h) show the separate contribution of up/downwelling, while panels (g,i) show the residual (net) water mass transformation rate. Note that the panels have all different x-axes.

Supplementary Files

This is a list of supplementary files associated with this preprint. Click to download.

- Mashayeketal21MountainstoclimbSUPPLEMENTARY.pdf